Theoretical Study of the Dynamics and Kinetics of the O + CS → CO + S Chemical Laser Reaction, where CO Shows a Very High Vibrational Excitation

Pablo Gamallo,[a] Rafael Francia,[b] Rodrigo Martínez,[b] Ramón Sayós,[a,*] and Miguel González[a,*]

[a]Departament de Química Física i IQTC, Universitat de Barcelona, C/ Martí i Franquès 1, 08028 Barcelona (Spain)

[b]Departamento de Química, Universidad de La Rioja, C/ Madre de Dios, 51, 26006 Logroño (Spain)

ABSTRACT

The dynamics and kinetics of the $O(^3P) + CS(X^1\Sigma^+) \rightarrow CO(X^1\Sigma^+) + S(^3P)$ chemical laser reaction was studied theoretically in detail for the first time, as a function of collision energy (0.0388-2.0 eV) and rovibrational excitation of CS. This was made using the quasi-classical trajectory (QCT) method and employing the best *ab initio* analytical ground potential energy surface ($1^3A'$ PES) available. A broad set of properties was determined, including scalar and vector properties, and the reaction mode. The behaviors observed and the considerable formation of OCS collision complexes were interpreted from some characteristics of the PES (early barrier, shallow minimum in the exit channel, and high exoergicity (mainly channeled into CO vibration; up to ≈81% of the available energy) and the kinematics. The QCT vibrational and rotational CO populations and the vector properties show a quite good agreement with experiments, but the QCT rate constants disagree. To better account for the kinetics, we performed CASPT2/aug-cc-pVTZ *ab initio* calculations on the stationary points along the minimum energy path of the ground and first excited ($1^3A''$) PESs. The transition state theory, which can be satisfactorily applied here, leads to rate constants (100-2000 K) that are quite close to the measured ones, where comparison is possible (150-300 K). We expect that these results will encourage further theoretical and experimental developments.

Keywords: O + CS, reaction, CO + S, chemical laser, kinetics, dynamics, quasi-classical trajectories, *ab initio* calculations, transition state theory.

Tables: 3 **Figures:** 9 **Proofs to**: Prof. Miguel González

***** Corresponding authors: r.sayos@ub.edu and miguel.gonzalez@ub.edu

Final revised version of the manuscript submitted to J Phys Chem A

I. INTRODUCTION

The reaction between atomic oxygen and carbon monosulfide[1]

$$O(^3P) + CS(X^1\Sigma^+) \rightarrow CO(X^1\Sigma^+) + S(^3P) \qquad \Delta_rH^\circ_{0K} = -3.76 \text{ eV} \quad (1)$$

is the primary source of vibrationally excited CO molecules in the carbon monoxide chemical laser, which was firstly observed by photolyzing a CS_2/O_2 mixture in a laser cavity.[2] This fact has motivated a considerable interest in the study of reaction (1), particularly from an experimental perspective.

The CO vibrational distribution, $P(v')$, at thermal reactant energies was determined by several groups using a variety of experimental techniques.[3,4,5,6,7,8,9] In these studies an important vibrational inversion was obtained and the maximum of the distribution was found at v'=12 or 13, with the vibrational levels populated up to the thermodynamic limit. The vibrational inversion is the main reason why this reaction can act as a laser medium. The CO rotational distributions, $P(v',j')$, at some of the most populated vibrational levels (v'=12-14) was measured by means of laser induced fluorescence (LIF), for thermal reactants (T=298 K) and for thermal CS (T=298 K) and hyperthermal oxygen atoms generated by photolysis of NO_2 at 355 nm.[10] An efficient conversion of reactants translational energy into rotational energy of CO was observed.

Some vector correlations of the title reaction were also studied experimentally (**kk'**, **kj'** and **k'j'** angles, where **k** and **k'** are the relative velocity of reactants and products, respectively, and **j'** is the rotational angular momentum of CO), using translational aligned oxygen atoms (formed from NO_2 polarized photolysis at 355 nm) and LIF detection of the nascent CO with sub-Doppler resolution.[11,12,13] This technique was applied for the first time to the $O(^3P) + CS \rightarrow CO + S$ and $O(^1D) + N_2O \rightarrow NO + NO$ reactions.[11] The CO molecule was produced with a small tendency to be forward or backward scattered, **j'** was preferentially perpendicular to **k'**, and **j'** was uncorrelated to **k**.

Regarding the kinetics, the rate constant appears to be rather well established for the reaction at room temperature, T~300 K, in units of $cm^3 \cdot mol^{-1} \cdot s^{-1}$: 13×10^{12} (298 K),[14] 12.4±0.84 ×

10^{12} (305 K),[15] 13.5±2.2 × 10^{12} (300 K),[16] and 12.9×10^{12} (294 K),[17] where the lowest and highest values measured at *T*=294 K in Ref. 17 were 9.6×10^{12} and 15.7×10^{12}, respectively. However, there is only a single set of experimental rate constant values as a function of temperature available (150-300 K interval).[17] The recommended rate constant (A=16.2$_6$ × 10^{13} $cm^3 \cdot mol^{-1} \cdot s^{-1}$ and E_a=6.55 10^{-2}±2.17 10^{-2} eV for *T*:150-300 K)[18] is based on the data of Ref. 17.

From a theoretical perspective there are only a few studies concerning the O + CS reaction (see, e.g., Refs. 19,20,21). This reaction was studied using the quasi-classical trajectory (QCT) method on a MNDO/CI analytical ground potential energy surface (PES),[19] the stationary points of the ground and first excited PESs (1^3A' and 1^3A", respectively) were analyzed by means of *ab initio* methods,[20] and an *ab initio* analytical ground PES was developed and employed in variational transition state theory rate constant calculations.[21]

In this work we investigated theoretically the scalar and vector dynamic properties and microscopic mechanism of the O + CS → CO + S reaction, using the QCT method[22,23,24,25] and employing the best *ab initio* analytical ground PES (1^3A') available (PES3 of Ref. 21). To the best of our knowledge, this is the first detailed theoretical study carried out on the dynamics of this reaction. Furthermore, in order to obtain a better description of the kinetics, transition state theory[26,27] rate constant calculations were performed, based on the transition states of the ground (1^3A') and first excited (1^3A") PESs determined here at the complete active space self consistent field and second order perturbation theory (CASPT2) *ab initio* level.[28,29,30]

The effect of the non-adiabatic interaction (intersystem crossing) between the 1^3A' and 1^3A" PESs and the singlet PESs that correlate with the O(^{1}D) + CS → CO + S(^{1}D) reaction, see, e.g., Ref. 31, is out of the scope of the present study. But the rather good agreement found between the theory and experiment (cf. section III) suggests that a description based on the 1^3A' and 1^3A" PESs is quite satisfactory, at least for the conditions where comparison with experiment is possible.

The paper is organized as follows: Section II describes the computational methods. Section III presents the PESs properties, TST and QCT rate constants, and QCT scalar and vector dynamic properties and the discussion. Finally, section IV gives the summary and conclusions.

II. COMPUTATIONAL DETAILS

Three adiabatic PESs, one of ^{3}A' symmetry and two of ^{3}A" symmetry, are involved in the title reaction.[20] On the reactants side the lowest energy ^{3}A' and ^{3}A" adiabatic surfaces come from avoided crossings between the diabatic surfaces arising from O(^{3}P)+CS($X^1\Sigma^+$) (ground state) and O(^{3}P)+CS($a^3\Pi$) (excited state). Similarly, on the products side they come from S(^{3}P)+CO($X^1\Sigma^+$) (ground state) and S(^{3}P)+CO($a^3\Pi$) (excited state).

Although the system can evolve on the three PESs indicated above, reactivity takes place mainly on the ground PES (1^3A'), which is always lying energetically below the 1^3A" PES. The analytical representation of the 1^3A' PES used in the QCT part of this study was reported in Ref. 21 and corresponds to the PES3 fit (many-body expansion function fit[32] of spin projected unrestricted fourth order Möller-Plesset (PUMP4) *ab initio* data (6-311G(2d) Pople's basis set)).

A*b initio* calculations at the second-order perturbation theory based on a zeroth-order CASSCF wave function (i.e., the CASPT2 method) were performed here to obtain a much better characterization of the barriers on the 1^3A' and 1^3A" PESs previously reported.[20,21] This was made using the standard correction, as implemented in MOLCAS 7.2.[33] We have checked several active spaces and the one comprising 14 electrons in 11 orbitals, CAS(14,11), was considered to be suitable for the present goal. In the calculations the two inner a' orbitals were kept frozen while five a' and one a" orbitals were defined as inactive. The rest of orbitals that comprise the active space (eight a' and three a" orbitals) generate 25396 and 25424 configuration state functions (CSFs) for the 1^3A' and 1^3A" PESs respectively.

On the other hand, the aug-cc-pVTZ correlation-consistent triple zeta basis set of Dunning was used in the present study, and supermolecule calculations were considered in the determination of the energies of the stationary points on each PES.

From Ref. 21 it comes out that for this reaction the conventional and variational transition state theory methods (TST and VTST methods, respectively)[26,27] lead to very similar results. That is to say, recrossing around the transition state is not playing a relevant role in this case. Thus, the TST method was used to calculate the rate constant, k_{TST}, for each PES, as a function of temperature, employing the well known expression:

$$k_{TST}(PES) = f_{el}\frac{k_B T}{h}\frac{Z_{\neq}^{'}}{Z_O Z_{CS}} e^{\frac{-E_o}{k_B T}} \qquad (2)$$

, where $Z_{\neq}^{'}$, Z_O and Z_{CS} are the partition functions for the transition state (excluding the part that corresponds to the motion along the reaction coordinate), O atom, and CS molecule, respectively, without including the electronic part. E_0 is the transition state energy with respect to reactants, taking into account the zero point energy (ZPE), and the other symbols have the usual meaning. Partition functions can be obtained for the ground and first excited PESs from the information provided in Table I.

The multiplicative term f_{el} in eq. (2) corresponds to the electronic term, which accounts for the weight of each PES on the total rate constant,

$$f_{el} = \frac{3}{5e^{-E(^3P_2)/k_B T} + 3e^{-E(^3P_1)/k_B T} + e^{-E(^3P_o)/k_B T}} \qquad (3)$$

and $E(^3P_2)$, $E(^3P_1)$ and $E(^3P_0)$ are the energies of the $^3P_2$, $^3P_1$ and $^3P_0$ spin-orbit levels of $O(^3P)$ relative to the ^3P electronic term (-9.66771 10^{-3}, 9.95481 10^{-3} and 1.847409 10^{-2} eV, respectively).[34]

Since the PESs calculations were performed without accounting for the spin-orbit coupling, the PESs correlate with reactants with the O atom without spin-orbit splitting (i.e., the O atom energy would correspond to the averaged energy of the spin-orbit splitted ^3P state). Hence, it makes

more sense to refer the energy of the spin-orbit levels of the O atom to the energy of the ^3P electronic term than to the spin-orbit level of lowest energy ($^3P_2$); see, e.g., Refs. 35 and 36.

On the other hand, if the tunneling contribution to reactivity is small, as it happens for this reaction at the temperatures of interest,[21] the Wigner expression can lead to a good estimate of tunneling. According to this equation the transmission coefficient (Γ) on each PES is given by

$$\Gamma = 1 + \frac{1}{24}\left[\frac{h|\nu_{imag}|}{k_B T}\right]^2 \left(1 + \frac{k_B T}{E_o}\right) \qquad (4)$$

, where $|\nu_{imag}|$ is the modulus of the imaginary frequency of the transition state, and the corrected values of the rate constants $k_{TST}(1^3A')$ and $k_{TST}(1^3A'')$, i.e., those including the tunneling correction, are Γ times the corresponding TST values.

The total rate constant k_{TST}, i.e., that including the contribution of the ground and first excited PESs to reactivity, is then obtained by

$$k_{TST} = k_{TST}(1^3A') + k_{TST}(1^3A'') \qquad (5)$$

where the rate constant on each PES was obtained using eqs. (2)-(4).

The QCT method was applied in the usual way[22,23,24,25] to the ground $^3A'$ analytical PES (PES3 fit).[21] The accuracy of the numerical integration of Hamilton's differential equations was verified by checking the conservation of total energy and total angular momentum for every trajectory. An integration step of 5.0×10^{-17} s and an initial distance of 10.0 Å between the O atom and the center of mass of the CS molecule were selected for each integrated trajectory. This separation ensures that the interaction energy is negligible compared to the available energy of reactants.

The rovibrational energy levels of the CS molecule were sampled according to a Boltzmann distribution at several temperatures selected in the interval 200-1500 K; and, for every chosen rovibrational temperature of CS (T_{vr}), the influence of the relative translational energy of reactants (E_T) was investigated within the interval 0.0388-2.0 eV. For each initial condition (E_T, T_{vr}) batches

of 1.5×10^5 trajectories were calculated in order to determine the cross sections and product state distributions on the ground PES. A similar number of trajectories was considered to determine the vibrational populations of CO arising from the reaction at T=300 K and to compare with the experimental data. The rovibrational levels of the CO product were assigned using the vibrational action angle variable method and employing the ordinary histogram binning, which for this system leads to the same results as the more refined Gaussian binning method.[37] Furthermore, for a selection of the initial conditions, 2.0×10^6 trajectories were run to calculate the vector properties. Finally, the QCT rate constant on the ground PES was obtained in the 100-2000 K temperature interval using batches of 2.5×10^5 trajectories at each temperature.

No reactive trajectories were found for the other possible channels (i.e., O + CS → SO + C and O + CS → O + C + S), due to the high energy requirement involved (2.18 and 7.06 eV, respectively).[21]

III. RESULTS AND DISCUSSION

A. STATIONARY POINTS OF THE PESs

The characteristics of the ground (1^3A') and first excited (1^3A") PESs of the highly exothermic O + CS → CO + S reaction are similar at the CASPT2/aug-cc-pVTZ level (CASPT2 level hereafter), as can be seen from the schematic representation of the energy profiles along the minimum energy path given in Figure 1, where it is also shown the energy profile of the 1^3A' analytical PES. The similarity of both PESs was already suggested in an earlier study of the stationary points,[20] where several *ab initio* methods were employed.

The CASPT2 geometry, harmonic vibrational frequencies and energy of the transition states (TSs) and shallow minima (MIN1 and MIN2) are reported in Table I. The different types of stationary points are quite similar to each other for both PESs, as indicated before. Besides, the

results for the ground PES obtained at the PUMP4/6-311G(2d) level (PUMP4 level hereafter) and in the analytical representation of this surface obtained from these *ab initio* calculations[21] are also reported in this table.

The properties of the diatomic molecules are also given in Table I. CASPT2 and experimental[38,39] results show a very good agreement in the case of the geometries and frequencies, and a quite good agreement for the reaction energy (the CASPT2 result agrees with the measured one if the experimental error margin is included). Analyzing the energies involved, i.e., examining the dissociation energies of the diatomic molecules, it comes out that D_o(CS)=7.57 eV and D_o(CO)=11.16 eV at the CASPT2 level, while the experimental values are 7.27±0.152 eV and 10.95±0.224 eV, respectively. Thus, the small difference found between the CASPT2 and experimental reaction energy values mainly comes from D_o(CS).

In the reactants valley the 1^3A' and 1^3A" PESs present a shallow O·····CS angular minimum of C_s symmetry, MIN1, situated -3.56 10^{-2} and -3.73 10^{-2} eV with respect to reactants (-2.65 10^{-2} and -2.65 10^{-2} eV if ZPE is taken into account) and with a reactants-like structure (Table I). In both surfaces this minimum connects, along the MEP and *via* a transition state, TS, with a shallow OC·····S angular minimum of C_s symmetry, MIN2, in the products valley.

The transition state corresponds to an early barrier, i.e., has a structure which is closer to reactants than to products, as expected for a strongly exothermic reaction. It has C_s symmetry and an OCS angle of 128.0º and 132.3º for the 1^3A' and 1^3A" surfaces, respectively, and with an energy barrier of 1.13 10^{-2} and 2.52 10^{-2} eV with respect to reactants, respectively (1.60 10^{-2} and 2.78 10^{-2} eV if ZPE is accounted for) (Table I). Therefore, although the barrier on the excited PES is small, it approximately doubles the value of the barrier on the ground PES.

It is very difficult to assess the accuracy of a high level *ab initio* method to determine energy barriers and, in addition, this depends on the reaction chosen. However, it is known that the CASPT2 method has a comparable accuracy as the MRCI+Q (Multireference Configuration

Interaction with Davidson correction) method for few electron systems,[40] and some details about the accuracy of the CASPT2 energies have been reported in the previous reference on the related O_2, SO and S_2 species (energies are accurate to at least 8.67 10^{-2} eV). The CASPT2 energy barriers obtained for reaction (1) are below this value but, due to the very strong exoergicity of this reaction, a very small barrier (or the absence of it) is expected, in consistency with the CASPT2 calculations. An additional insight into the suitability of the CASPT2 barriers can be found in section III.B, where the rate constants are reported.

The shallow products valley minimum MIN2 is placed -5.81 10^{-2} and -6.16 10^{-2} eV with respect to products (-5.16 10^{-2} and -5.55 10^{-2} eV if ZPE is included), for the 1^3A' and 1^3A" surfaces, respectively, and has a products-like structure (Table I). From this minimum the products can be reached without surmounting any barrier on the MEP (Figure 1). MIN2 plays a considerable role in the reaction, as it will be shown in section III.F, where the reaction mode on the analytical ground PES[21] was analyzed using the QCT method.

The PUMP4 ground PES results are in general similar to those obtained here at the CASPT2 level, with the later ones being more accurate. For the CS and CO diatomic molecules the PUMP4 method tends to produce somewhat larger equilibrium distances and vibrational frequencies than the experimental ones. The CASPT2 method practically matches the experimental values for both the geometry and frequencies.

The analytical expression of the 1^3A' PES,[21] which was build up from a set of about 800 PUMP4 points, reproduces quite satisfactorily the *ab initio* data and, in particular, the transition state, reactants and products properties. However, in Ref. 21 the barrier height of the analytical surface was scaled (from 9.80 10^{-2} eV at the PUMP4 level to 3.69 10^{-3} eV in the analytical PES) to try to reproduce theoretically (variational transition state calculations) the experimental rate constant at 300 K. From the CASPT2 method a value of 1.13 10^{-2} eV (1.60 10^{-2} eV including the ZPE) has been obtained for the 1^3A' PES barrier and, although the geometry is similar to that of the

analytical surface, the CO separation is about 0.2 Å larger and the bending frequency is substantially smaller than in the analytical surface and PUMP4 calculations. Consequently, the CASPT2 transition state resembles the reactants even more than the previous calculations.

The previous 1^3A' PES[21] also presents a shallow minimum in both the reactants (MIN1) and products (MIN2) regions. However, they were not investigated in that work as they were considered to be unimportant due to their very small depth (the energies of MIN1 and MIN2 are -3.34 10^{-2} and -3.95 10^{-2} eV with respect to reactants and products, respectively). However, in order to improve the characterization of the analytical ground PES,[21] which will be used later on in the QCT calculations, here we have located both shallow minima and a transition state that connects the minimum of the exit valley with products (Table I). As we have seen before, at the higher level CASPT2 *ab initio* calculations the transition state in the exit valley was not found (Figure 1).

It is suitable to discuss here the possible implications on the reaction dynamics arising from the differences between the CASPT2 and the analytical 1^3A' PES properties. But before doing this it will be useful to take into account the QCT results obtained here employing the LEPS (London-Eyring-Polanyi-Sato) model PES reported in Ref. 13, which was constructed using experimental data. In all we have calculated 400 000 trajectories on the LEPS PES for E_T=0.075 and 2.0 eV and T_{vr}=300 and 1500 K.

The LEPS cross section is much larger than that of the analytical 1^3A' PES one at E_T=0.075 eV, but both cross sections are similar at E_T=2.0 eV. The higher LEPS reactivity, which is particularly evident at low E_T, comes from its too small energy barrier.[13] The LEPS vibrational distribution of the CO molecule produced in the reaction at T=300 K is similar although broader than the 1^3A' PES one (cf. section III.D). The LEPS vector properties are rather similar to the 1^3A' PES ones and, in addition, long- and short-lived OCS collision complexes are formed in the products valley of the LEPS surface at 0.075 eV (59 and 53% at 300 and 1500 K, respectively, and 34 and 36% at 300 and 1500 K, respectively). At 2.0 eV the reaction mainly occurs in a direct way

(89 and 91% at 300 and 1500 K, respectively). These results on the microscopic reaction mechanism are on the overall similar to those obtained for the 1^3A' PES (cf. section III.F).

Hence, although the shape of the LEPS model PES is quite different from that of the analytical 1^3A' PES (and leaving out the too small LEPS energy barrier), on the overall the dynamic results obtained from both PESs are similar. This suggests that the reaction dynamics at low-moderate collision energies is mainly determined by the strong exothermic character of the reaction and by the heavy-heavy-heavy kinematics.

From the results of the previous comparison and taking into account the differences between the analytical 1^3A' PES and the CASPT2 stationary points, we think than the main effects on the properties calculated using this PES will occur for the reactivity and the relative importance of the collision complexes in the reaction mode.

The reaction energy on the analytical 1^3A' PES (-3.93 and -3.88 eV without including the ZPE and including it, respectively) is only somewhat larger (in absolute value) than the CASPT2 one (-3.65 and -3.59 eV, respectively). Moreover, even though the energy barrier with respect to reactants is really small in both the analytical 1^3A' PES ($3.69\ 10^{-3}$ and $1.56\ 10^{-2}$ eV without including the ZPE and including it, respectively) and the CASPT2 calculations ($1.13\ 10^{-2}$ and $1.60\ 10^{-2}$ eV, respectively), the QCT cross section on the former is expected to be larger than that resulting from a PES reproducing the CASPT2 barrier, especially at the lower E_T values explored. A shift of the present QCT excitation function (cross section vs collision energy; cf. section III.C) of about $7.61\ 10^{-3}$ eV toward higher E_T values can reasonably be expected.

Moreover, the importance of the collision complexes (in particular the long-lived ones) in the microscopic mechanism on the analytical 1^3A' PES will probably be less than indicated (cf. section III.F), due to the presence of a barrier of $19.0\ 10^{-2}$ eV between the product valley minimum and the reaction products which does not appear in the CASPT2 calculations (Figure 1).

Furthermore, the products valley minimum on the analytical PES (-3.95 10^{-2} eV respect to products) is less deep than in the CASPT2 calculations (-5.81 10^{-2} eV respect to products).

In spite of the differences found between the analytical 1^3A' PES and the CASPT2 calculations and, as indicated above in the comparison with the LEPS model PES, in our view the dynamic properties at low-moderate energies are mainly controlled by the reaction exothermicity and kinematics. Hence, in our opinion the analytical PES 1^3A' used here, which is the best available one to be used in dynamic calculations, is probably able to describe this system reasonably well under those reaction conditions.

B. RATE CONSTANTS

Before showing the results of the rate constants calculations, it should be noted than the transition states of the 1^3A' and 1^3A" PESs, TS(1^3A') and TS(1^3A"), respectively, really connect MIN1(1^3A') with MIN2(1^3A') and MIN1(1^3A") with MIN2(1^3A"), respectively; and not the O + CS reactants with the CO + S products. Nevertheless as these shallow MIN1 and MIN2 minima are very close in geometry and energy to reactants and products, respectively, (Table I), the use of the TS(1^3A') and TS(1^3A") properties to calculate, according to TST, the O + CS → CO + S rate constants on the 1^3A' and 1^3A" PESs, respectively, is a good approximation.

From the CASPT2 reactants and transition state structure, harmonic vibrational frequencies and energy and according to equations (2)-(4), we calculated the rate constants of the ground and excited PESs (k_{TST}(1^3A') and k_{TST}(1^3A"), respectively), and the total rate constant (k_{TST}) (eq. (5)) in a wide interval of temperatures (T=100-2000 K). These results are presented in Table II and Figure 2 (Arrhenius's plots that show noticeable curvatures), together with the experimental data and other theoretical results.

k_{TST}(1^3A') is greater than k_{TST}(1^3A") from T=100 to 250 K (k_{TST}(1^3A')/k_{TST}(1^3A") ratio of 2.69 and 1.07, respectively), they are nearly identical at T=275 K, and k_{TST}(1^3A") is greater than

$k_{TST}(1^3A')$ from T=300 to 2000 K ($k_{TST}(1^3A'')/k_{TST}(1^3A')$ ratio of 1.04 and 1.61, respectively). Hence, the ground PES is more reactive than the excited PES only below T=250 K. k_{TST} increases with T, as expected for a reaction with barrier. Thus, in the T=100-300 K interval k_{TST} increases a factor of 16.4, while in the T=300-2000 K interval it increases a factor of 12.8. This moderate growth arises from the small barriers found on the ground and excited PESs.

The tunnel effect influence on reactivity is small, with the only exception of what happens at the lowest temperature investigated (T=100 K), as can be anticipated for a three heavy atoms reaction. This low tunneling contribution is due to the small value of the modulus of the imaginary frequency of the transition state in both the ground and excited PESs. The maximum tunnel effect occurs at T=100 K, as expected, where it contributes as 11% and 18% for $k_{TST}(1^3A')$ and $k_{TST}(1^3A'')$, respectively. At T=300 K the tunneling contribution becomes smaller (4% and 7% for the ground and excited states) and, finally, at T=1000 K it reaches a percentage of only 1 % and 2 %, respectively. The larger contribution of tunneling to $k_{TST}(1^3A'')$ in comparison to $k_{TST}(1^3A')$ comes from the larger imaginary frequency of TS($1^3A''$) in comparison to that for TS($1^3A'$) (378.5i cm^{-1} vs 214.4i cm^{-1}, respectively (cf. CASPT2 values in Table I)).

Before comparing the TST results with the experimental data it is worth remembering here that the recommended values for the O + CS → CO + S rate constant[18] are based on a single set and rather old experimental data,[17] where the rate constant was measured in the T=150-300 K interval.

The TST rate constant, $k_{TST,}$ is close (or very close) to the experimental rate constant, k_{exp}, in the full interval of temperature where measurements were made, if we take into account the experimental error margins (Table II and Figure 2). Leaving out the error bars, the k_{TST}/k_{exp} ratio takes the following values 2.06, 1.48, 1.18, 1.00, 0.88, 0.81, and 0.75 at the temperatures of 150, 175, 200, 225, 250, 275 and 300 K, respectively. The CASPT2 TST rate constant values are the best theoretical results available and show a much better agreement with the experiment than previous investigations (VTST calculations based on the analytical PES employed here[21] and QCT

calculations on a MNDO/CI based analytical PES ($1^3A'$)[19]); cf. Table II and Figure 2.

The Arrhenius plot shows curvature and because of this we considered separately the 100-300 K and 300-1000 K temperature intervals, for which we obtained the following pre-exponential factor (A) and activation energy (E_a) results: $A=3.62\times10^{13}$ $cm^3\cdot mol^{-1}\cdot s^{-1}$ and $E_a= 3.59\ 10^{-2}$ eV, and $A=10.8\times10^{13}$ $cm^3\cdot mol^{-1}\cdot s^{-1}$ and $E_a= 6.53\ 10^{-2}$ eV, respectively. The recommended experimental values in the 150-300 K temperature range are $A=16.2_6\times10^{13}$ $cm^3\cdot mol^{-1}\cdot s^{-1}$ and $E_a= 6.55\ 10^{-2}\pm2.17\ 10^{-2}$ eV.[18]

Regarding the QCT rate constant calculations performed here, which also include the electronic factor of eq. (3), these results are in general very similar to the TST results determined on the same analytical ground PES[21] (Table II). This can be understood on the basis of the little influence of tunneling and recrossing on reactivity already mentioned.

C. CROSS SECTIONS

The dependence of the cross section (σ) as a function of collision energy and for selected values of T_{vr} (300, 1000 and 1500 K) is shown in Figure 3. The QCT cross section strongly increases with E_T in the 0.0388-0.1 eV range, a moderate increase is obtained in the 0.1-0.5 eV interval, and, finally, the increase becomes rather less intense above 0.5 eV. Furthermore, a plateau is reached at about 2.0 eV.

The raise of σ with E_T mainly results from the increase of the average reaction probability, $\langle P_r \rangle$, with E_T, as b^2_{max} is independent of E_T from 0.5 to 2 eV ($\sigma(QCT) = \pi\, b^2_{max}\langle P_r \rangle$, where b_{max} and $\langle P_r \rangle$ are the maximum impact parameter and the reaction probability averaged over the range of impact parameters, respectively). Moreover, from 0.0388 to 0.5 eV b_{max} decreases from ≈4 Å to ≈3 Å. Differing from what happens in the case of collision energy, the thermal rovibrational excitation of CS has a slight effect on the cross section (Figure 3).

The cross section behavior can be rationalized on the basis of the characteristics (early barrier) of the transition state of the ground PES (early barriers are expected for strongly exoergic reactions like the one studied here). This makes the relative translational energy (collision energy) to be particularly efficient for the reactants to overcome the barrier and evolve into the products valley and, in addition, reactants relative translational energy tends to be transformed into vibrational energy of products (Polanyi's rules).[41] The energy distribution in CO + S products will be considered below.

D. PRODUCT STATE DISTRIBUTIONS

The average fractions of translational, vibrational and rotational energy in products ($\langle f_T' \rangle$, $\langle f_V' \rangle$, and $\langle f_R' \rangle$, respectively) are useful to obtain an overall perspective of the energy partitioning in products, and they are given in Table III for E_T=0.075, 0.3, 1.0 and 2.0 eV and T_{vr}=300 and 1500 K. The $\langle f_V' \rangle$ fraction is always larger than $\langle f_T' \rangle + \langle f_R' \rangle$ and $\langle f_V' \rangle$ decreases from ≈81% of the available energy (E_{av}) at the lowest E_T (0.075 eV) up to ≈55% of E_{av} at the highest E_T (2.0 eV); i.e., even at high collision energies, the reaction is a source of CO molecules with vibrational excitation, and, in addition, the rovibrational temperature of CS has a minor influence on the average energy fractions. By the contrary, both the $\langle f_T' \rangle$ and $\langle f_R' \rangle$ fractions increase with collision energy, as expected and as it was also found in the experiments.[10] The lowering of $\langle f_V' \rangle$ with collision energy increasing comes from the progressively higher difficulty for the O + CS system to evolve into the CO + S products following the minimum energy path.

The data reported in Table III were calculated taken into account the ZPE of CO. If this energy is not considered essentially the same average fractions are obtained. It goes like this because the ZPE represents a small amount of energy compared to the available energy of products and the CO product molecule is formed with a very high vibrational excitation. Thus, e.g., the

largest difference observed between both sets of results (i.e., with and without including the ZPE of CO) for $\langle f_V' \rangle$ is below 2.0 % (0.54 vs 0.53 for E_T=2.0 eV and T_{vr}=1500 K).

More detailed information on the energy distribution of products can be obtained from the vibrational populations of CO ($P(v')$). The QCT vibrational distributions for selected E_T values [0.075, 0.3, 1.0 and 2.0 eV] and T_{vr} values of CS (300, 1000 and 1500 K) are shown in Figure 4. In all cases the vibrational distributions are inverted, with the more populated levels placed in the interval v'=11-13. The most populated vibrational level of CO is v'=13 except for the highest collision energy, E_T =2.0 eV, where the vibrational levels in the range around $10 \leq v' \leq 13$ present similar populations. The vibrational inversion observed is a necessary condition to consider the title reaction as a convenient laser medium. Furthermore, the generation of vibrational excited products is likely to occur in a reaction that takes place on a PES with an early barrier.[41]

When E_T increases the distribution becomes broader, as expected. Thus, e.g., in the case of E_T =2.0 eV all vibrational levels within the interval $4 \leq v' \leq 20$ are populated. The influence of the CS rovibrational temperature in the CO vibrational distributions is really small, and the distributions are very close to each other for all T_{vr} explored.

To compare with the experiments, we also calculated the vibrational distribution of CO arising from thermal O + CS reactants at T=300 K (Figure 5). The QCT distribution is presented in this figure together with the experimental data[3] and the results of a previous QCT investigation using an empirical analytical PES.[10] The agreement is rather good with the maximum of the present QCT and experimental $P(v')$ distributions peaking at v'=13, as it happens in most of the E_T and T_{vr} conditions analyzed in this work. Similar results were also reported in earlier QCT calculations of our own based on a semiempirical MNDO/CI analytical PES.[19]

The QCT $P(v')$ distribution obtained here at T=300 K is narrower than the experimental one and the origin of this difference is unclear, although, in principle, it could be attributed to the PES. We should note, however, that broader QCT $P(v')$ distributions are found when higher energies are

involved (cf. Figure 4) and, on the other hand, LIF measurements of vibrational distributions have larger uncertainties than those based on IR (infrared) techniques.

For the more populated vibrational levels of CO (v' =12-14) we determined the rovibrational distributions ($P(v',j')$) at selected values of E_T and T_{vr}. The most populated j' value becomes smaller as v' is greater. This is the expected behavior for a triatomic reaction, where more vibrational excitation correlates with less rotational excitation and vice versa. The increase of E_T keeping constant T_{vr} increases $<j'>$ for each vibrational level, in agreement with the experiments,[10] and the increase of T_{vr} keeping constant E_T also increases $<j'>$.

Figures 6a and 6b show the comparison between the QCT $P(v',j')$ results obtained here at T=300 K (i.e., both E_T and T_{vr} correspond to a thermal distribution of O + CS at T=300 K), and the experimental values for v'=12 and 14.[10] The agreement is rather good for v'=12 but a shift toward higher j' values is observed in the QCT distributions for v'=14 (and this also happens for v'=13). Furthermore, in Figures 6c and 6d, we present the experimental results at T_{vr}=300 K and a higher translational energy[10] (E_T distribution with peaks at 0.13 and 0.26 eV) with the QCT values found at T_{vr}=300 K and two different collision energies (E_T= 0.1 and 0.2 eV). The QCT distributions at 0.1 and 0.2 eV are rather similar to each other for both CO vibrational levels and similar to the experimental data.

Thermal rotational distributions of CO plotted in Figures 6a-6b were derived taken as a reference the most populated QCT j' value and obtaining the "associated" temperature value from equation (5) (rigid rotator model), where the equilibrium rotational constant B_e is given in wave numbers:

$$j_{max} = \sqrt{\frac{k_B T}{2 B_e hc}} - \frac{1}{2} \qquad (5)$$

E. TWO- AND THREE-VECTOR CORRELATIONS

After the QCT study of the scalar properties of O + CS → CO + S on the ground PES, we investigated its vector properties (stereodynamics), considering the two-vector angular distributions **kk'**, **kj'** and **k'j'** (where **k** and **k'** correspond to the initial and final relative velocity vectors, respectively, and **j'** refers to the rotational angular momentum vector of CO), and the three-vector angular distribution associated to the **kk'j'** dihedral angle.

The **kk'** angular distribution was given in terms of the differential cross section per unit of solid angle, $d^2\sigma/d\Omega$ (DCS), and using its dimensionless form ($2\pi/\sigma$ times the $d^2\sigma/d\Omega$ value; relative DCS); and the **kj'** and **k'j'** angular distributions were specified in terms of the probability density function [P(**kj'**) and P(**k'j'**), respectively].[42] Typical examples of these distributions for the title reaction are given in Figures 7a-7f. Moreover, the **kk'j'** dihedral angle distribution was expressed in terms of the probability density function P(**kk'j'**)[42] (Figures 8a-8b)**.**

The **kk'** angular distribution is rather isotropic, particularly at E_T=0.075 eV, and with some tendency towards forward scattering, this behavior being more evident as collision energy increases (Figures 7a-7b). Of course, in spite of the presence of a peak at very small scattering angles, this does not correspond to a stripping-like mechanism for the C atom transfer from the CS molecule to the attacking O atom, because backward scattering is also important. The forward/backward scattering ratio, expressed as DCS(0-90^o)/DCS(90-180^o), is equal to 0.91, 1.49, 1.80, and 1.72 for E_T=0.075, 0.3, 1.0, and 2.0 eV (T_{vr}=300 K), respectively; and similar but less forward results are obtained at T_{vr}=1500 K (0.83, 1.32, 1.68, and 1.67, respectively). The results for E_T=0.075 and 0.3 eV and T_{vr}=300 K are consistent with the superthermal experimental data (where the E_T distribution peaks at 0.13 and 0.26 eV and T_{vr}=300 K),[13] which show a small propensity of the CO product to be forward or backward scattered.

The trend to a rather isotropic **kk'** distribution (leaving out the peak at very small scattering angles mentioned above) probably comes from the low barrier and moderate anisotropy of the

PES,[21] together with the heavy-heavy-heavy (H-H-H) kinematics of the system and the large amount of energy that appears as internal energy of products, which make easier for the system to remain during sometime around the shallow minimum structure of the products valley (cf. reaction mode in section F). The formation of collision complexes will also probably affect the other vector properties examined, although its influence has not been investigated here because it is not an objective of this study.

The **kj'** angular distribution (Figures 7c-7d) is symmetric around 90º, as it must be as a result of the invariance of the distribution of the CO product molecular axis by reflection on the **kk'** plane.[42] This distribution is rather broad and presents different shapes, which mainly depend on E_T and to a less extent on T_{vr}. While a maximum of P(**kj'**) occurs at 90º for E_T=0.075 and 0.3 eV, the situation is very different for E_T=1.0 and 2.0 eV, where maximum P(**kj'**) values are achieved at 0º and 180º. The small correlation found between **k** and **j'** for E_T=0.075 and 0.3 eV at T_{vr}=300 K contrasts a bit with superthermal experimental data[13] where, within the precision of the measurements, **j'** is uncorrelated to **k**.

Direct exam of the angular momentum vectors for reactive trajectories shows that contribution of **l** to the total angular momentum **J** (**J** = **l** + **j** = **J'** = **l'** + **j'**) is larger or much larger than the contribution of **j** (<|**l**|>/<|**j**|> = 2.2 and 11.9 for E_T = 0.075 and 2.0 eV, respectively; T_{vr}=300 K), while the contribution of **l'** to **J** is larger than that of **j'** (<|**l'**|>/<|**j'**|> = 1.8 and 3.1, respectively), with **l** and **l'** being similar (<|**l**|>/<|**l'**|> = 0.8 and 1.0 and <**ll'**> = 40.7 and 19.2º, respectively).

Furthermore, there is a weak correlation between **j'** and **l** and between **j'** and **l',** with the exception of what happens at 0.075 eV where there is a preference for large **l'j'** angles. At 2.0 eV there is a smaller trend to populate large and small **l'j'** angles, but the associated solid angles lead to the peak at 90º observed for P(**k'j'**) at 0.075 and 2.0 eV that will be discussed below. Regarding the **lj'** angle there is a somewhat less tendency to obtain small and large values when evolving from

0.075 to 2.0 eV, decreasing in this way the importance of P(**kj'**) at 90º as E_T increases.

To understand the P(**kj'**) distribution is probably better to investigate the correlation between the **kj'** and **kk'** angles. In fact, at E_T=0.075 eV and T_{vr}=300 K there is a weak correlation between both angles, although for **kk'**<60º and **kk'**>120º there is a progressive preference for **kj'** being around 90º, as **kk'** decreases and increases, respectively. However, at E_T=2.0 eV and T_{vr}=300 K for **kk'**<40º the **kj'** angle is rather peaked around 90º, while for 40º<**kk'**<120º there is a progressive tendency to produce **kj'** at small and high angles, as **kk'** increases; and the intensity of this behavior is amplified in P(**kj'**) due to the associated **kj'** solid angles.

The **k'j'** angular distribution (Figures 7e-7f) has a symmetric shape around 90º, as it must be due to the reflection symmetry in the scattering plane (**kk'** plane).[42] This distribution is less broad than the **kj'** one and presents somewhat different shapes, mainly depending on E_T. A maximum of P(**k'j'**) occurs at 90º essentially for all reaction conditions investigated, this being particularly evident for E_T=0.075 and 0.3 eV at T_{vr}=300 K. This result is consistent with superthermal experimental data,[13] where the CO product is observed to be formed with **j'** preferentially perpendicular to **k'**. This behavior has been interpreted above in terms of the **l'j'** distribution, and the simpler evolution of P(**k'j'**) with E_T as compared to that for P(**kj'**) is easy to understand. Thus, at E_T=0.075 and 2.0 eV and T_{vr}=300 K the **kj'** angles are peaked at 90º for all the **kk'** angular interval.

Up to now the results obtained suggest that the reaction mode of the title reaction is mainly of direct type, and this is also corroborated by the P(**kk'j'**) data (Figures 8a-8b). The ϕ angle (or **kk'j'** angle) is the dihedral angle arising from the plane defined by vectors **k'** and **j'** with respect to the plane defined by vectors **k** and **k'**. Its interest in reaction dynamics was revealed in the pioneer work of Herschbach and coworkers on statistical long-lived complex-forming reactions.[43] Figures 8a-8b show that there is a preference of the rotational angular momentum vector of CO to be

perpendicular to the scattering plane (ϕ=90º and 270º) at low-moderate E_T (0.075 and 0.3 eV) and especially at the lower T_{vr} (300 K), where there is also a significant symmetry around 180º.

F. MICROSCOPIC REACTION MECHANISM

The reaction mode of O + CS → CO + S on the ground PES was analyzed for low and high collision energies (E_T=0.075 and 2.0 eV, respectively) at rovibrational temperatures of CS of 300 and 1500 K. To do this, for each initial condition selected, we considered representative samples of reactive trajectories; and for each one of them we analyzed the time evolution of the O-C, C-S and S-O internuclear distances.

The different types of reactive trajectories found are shown in Figure 9, where the collision complexes are formed around the structure of the products valley minimum of the PES.[21] The long-lived collision complexes have a lifetime equal or larger than ≈0.3 ps and values up to ≈2 ps were found at E_T=0.075 eV and T_{vr}=300 K. The short-lived collision complexes have smaller lifetimes than the long-lived ones and values up to ≈0.04 ps were found at E_T=2.0 eV.

At low collision energy (E_T=0.075 eV) the formation of long- and short-lived collision complexes is by far the preferred microscopic mechanism of the O + CS reaction. Thus, the percentage of reactive trajectories occurring through long-lived collision complexes (Figure 9c) are 44 and 30% for T_{vr}=300 and 1500 K, respectively; whereas the formation of short-lived collision complexes (Figure 9b) corresponds to 40 and 31% for 300 and 1500 K, respectively. Finally, the percentage of reactive events that take place *via* a direct microscopic mechanism (Figure 9a) is 16 and 39% at T_{vr}=300 and 1500 K, respectively.

At high collision energy (E_T=2.0 eV) the O + CS reaction mainly occurs in a direct way for all temperatures studied (86 and 85% for T_{vr}=300 and 1500 K, respectively). However, a competitive mechanism, involving the formation of short-lived collision complexes, has a small but not negligible contribution to reactivity (14 and 15% for T_{vr}=300 and 1500 K, respectively).

Hence, as collision energy increases the implication of collision complexes in the reactivity decreases, as expected. The effect to the rovibrational temperature of CS is very small at the higher collision energy investigated, while is playing a role at the lower one. Thus, the participation of collision complexes in the reactive processes tends to diminish as T_{vr} increases.

The formation of collision complexes may be somewhat enhanced by the presence of a barrier connecting the products valley minimum with products on the analytical ground PES, which is not present in the CASPT2 calculations (cf. section III.A and Table I). However, the influence of the products valley minimum in what refers to the formation of collision complexes appears to be clear.

The types of trajectories found in the case of the reactive scattering are also found in the non-reactive one (see, e.g., Figure 9d), but the relative weight of each type is different. Thus, e.g., for E_T=0.075 eV and T_{vr}=300 K, ≈98% of the non-reactive trajectories are reflected into reactants with -0.03 < V_{min} < 0.00 eV. V_{min} is the minimum potential energy value observed during the evolution of the trajectories and the energies are given with respect to reactants, as usual. Only ≈2% of the non-reactive trajectories satisfy that -3.97 < V_{min} < -3.03 eV, i.e., reach geometries around the products valley minimum (potential energy of -3.97 eV) before being reflected into reactants. By the contrary, the reactive trajectories (-3.97 < V_{min} < -3.93 eV in all cases reach geometries around the products minimum, before leading to products. The results obtained for E_T=0.075 eV and T_{vr}=1500 K are essentially coincident with the previously indicated.

For E_T=2.0 eV and T_{vr}=300 K, ≈90% of the non-reactive trajectories are reflected into reactants with -0.17 < V_{min} < 0.00 eV and ≈10% of them satisfy that -3.97 < V_{min} < -2.05 eV before being reflected into reactants. The reactive trajectories (-3.97 < V_{min} < -3.93 eV) in all cases reach geometries around the products minimum, as for E_T=0.075 eV. The results obtained for E_T=2.0 eV and T_{vr}=1500 K are essentially the same as those for E_T=2.0 eV and T_{vr}=300 K.

IV. SUMMARY AND CONCLUSIONS

The dynamics of the $O(^3P) + CS(X^1\Sigma^+) \rightarrow CO(X^1\Sigma^+) + S(^3P)$ reaction was studied as a function of E_T (0.0388-2.0 eV) and T_{vr} of CS (300-1500 K), and also at T=300 K; besides, the kinetics was also analyzed at thermal conditions (T:100-2000 K). To the best of our knowledge, this is the first detailed theoretical study on this reaction and was made applying the QCT method on the best *ab initio* analytical ground PES available (PES3 of Ref. 21).

Moreover, to improve the description of the minimum energy path of the two main PESs of the system (ground ($1^3A'$) and first excited ($1^3A''$) surfaces), additional *ab initio* calculations at the CASPT2 level were performed, and the results were used to investigate the kinetics by means of the transition state theory, which can be satisfactorily applied to this system.[21]

A wide set of dynamic observables were determined with the QCT method, including scalar properties (cross sections and product state distributions), vector properties (angle distributions involving the **kk'**, **kj'** and **k'j'** vectors and dihedral angle distribution of **kk'j'**), and the microscopic reaction mechanism. The behavior observed in both type of properties and the considerable formation of OCS collision complexes can be rationalized taking into account some characteristics of the $1^3A'$ PES (early barrier, shallow minimum in the products valley, and high exoergicity (-3.93 eV on the analytical PES, which is mainly channeled into CO vibration)) and the H-H-H kinematics of the system.

The most remarkable property we can mention is the very high fraction of available energy that appears as vibration of CO. At T_{vr}=300 K $\langle f_V' \rangle$=0.81, 0.79, 0.70, and 0.55 for E_T=0.075, 0.3, 1.0, and 2.0 eV, respectively; and the results are essentially the same at T_{vr}=1500 K. This very high vibrational energy content is also reflected in the CO vibrational distribution which peaks at v'=13 irrespective of the initial condition explored, although as translational energy increases the $P(v')$ distributions become wider, as expected.

The QCT vibrational and rotational populations of CO show a quite good agreement with the experiments,[3,10] (although the QCT $P(v')$ distribution from the reaction at T=300 K is narrower than the experimental one), and the vector properties are consistent with the experimental evidences.[13] However, the QCT rate constant values obtained on the ground PES suggest (taking into account the similarity of the ground and first excited PESs) that the calculations on both PESs should lead to lower rate constants than the experimental ones, which were measured in the 150-300 K temperature range.[17,18]

To better account for the main PESs and kinetics, we performed *ab initio* CASPT2/aug-cc-pVTZ calculations to locate the transition states of the $1^3A'$ and $1^3A''$ PESs. The resulting TST rate constants, taking into account the contributions of both surfaces, are quite close to the measured data. Thus, based on this good agreement, we believe that the TST data obtained here can be useful to describe the kinetics of the O + CS reaction in the wide T interval (100-2000 K).

Even though the differences found between the *ab initio* analytical ground PES and the CASPT2 stationary points, we think that at low and moderate energies the dynamic properties are mainly governed by the large exothermicity of O + CS → CO + S and the kinematics and, due of this, the PES provides a reasonably good description of the reaction dynamics under these conditions.

We expect that the present results on the main potential energy surfaces and on the dynamics and kinetics of this interesting chemical laser system will encourage further theoretical work, in particular on the O(^{3}P) + CS and O(^{1}D) + CS PESs and non-adiabatic couplings between them. Furthermore, experimental work on these reactions using molecular beam techniques and additional measurements on the dependence of the rate constant on the temperature are also desirable.

ACKNOWLEDGMENTS

This work was supported by the Spanish Ministry of Science and Innovation (MICINN projects CTQ2008-06805-C02-01, CTQ2011-27857-C02-01 and CTQ2009-07647). Thanks are also given to the "Generalitat de Catalunya" (Autonomous Government of Catalonia; ref. 2009SGR 17 and XRQTC) for some help.

TABLES

Table I. *Ab initio* and experimental results for the $1^3A'$ and $1^3A''$ OCS PESs stationary points.

	R_e(OC) / Å	R_e(CS) / Å	<OCS / ^{o}	ν_i / cm^{-1} [a]	E / eV [b]
$O(^3P)+CS(X^1\Sigma^+)$					
PUMP4 [c]	---	1.5645	---	1449.5 ($8.99\ 10^{-2}$)	0.0 (0.0)
CASPT2	---	1.5446	---	1273.9 ($7.90\ 10^{-2}$)	0.0 (0.0)
Analytical PES [c]	---	1.5645	---	1448.4 ($8.98\ 10^{-2}$)	0.0 (0.0)
Experimental [d]	---	1.5349	---	1285.1 ($7.97\ 10^{-2}$)	0.0 (0.0)
MIN1 ($1^3A'$) [f]					
CASPT2	2.9592	1.5439	158.7	1293.5 54.87 72.72 ($8.81\ 10^{-2}$)	$-3.56\ 10^{-2}$ ($-2.65\ 10^{-2}$)
Analytical PES [c]	3.6685	1.5645	85.9	1446.5 62.43 94.90 ($9.94\ 10^{-2}$)	$-3.34\ 10^{-2}$ ($-2.39\ 10^{-2}$)
MIN1 ($1^3A''$)					
CASPT2	2.9375	1.5434	161.2	1296.3 62.20 87.90 ($8.97\ 10^{-2}$)	$-3.73\ 10^{-2}$ ($-2.65\ 10^{-2}$)
TS ($1^3A'$)					
PUMP4 [c]	2.0888	1.5566	126.6	479.0i 184.3 1299.5 ($9.20\ 10^{-2}$)[g]	$9.80\ 10^{-2}$ ($10.0\ 10^{-2}$)
CASPT2	2.2885	1.5452	128.0	214.4i 86.62 1262.2 ($8.36\ 10^{-2}$)	$1.13\ 10^{-2}$ ($1.60\ 10^{-2}$)
Analytical PES [c]	2.0760	1.5553	126.8	177.4i 252.4 1389.3 ($10.2\ 10^{-2}$)	$3.69\ 10^{-3}$ ($1.56\ 10^{-2}$)
TS ($1^3A''$)					
CASPT2	2.2934	1.5425	132.3	378.5i 47.28 1267.0 ($8.15\ 10^{-2}$)	$2.52\ 10^{-2}$ ($2.78\ 10^{-2}$)
MIN2 ($1^3A'$) [f]					
CASPT2	1.1324	3.3579	168.9	2166.5 40.49 61.04 ($14.1\ 10^{-2}$)	-3.70 [h] (-3.64)
Analytical PES [c]	1.1437	2.5960	123.7	2262.9 351.9 150.9 ($17.1\ 10^{-2}$)	-3.97 (-3.89)
MIN2 ($1^3A''$)					
CASPT2	1.1325	3.3435	171.5	2166.7 28.44 63.22 ($14.0\ 10^{-2}$)	-3.71 [h] (-3.65)
$S(^3P)+CO(X^1\Sigma^+)$					
PUMP4 [c]	1.1436	---	---	2291.9 ($14.2\ 10^{-2}$)	-3.93 (-3.88)
CASPT2	1.1328	---	---	2162.7 ($13.4\ 10^{-2}$)	-3.65 (-3.59)
Analytical PES [c]	1.1436	---	---	2291.3 ($14.2\ 10^{-2}$)	-3.93 (-3.88)
Experimental [d,e]	1.1283	---	---	2169.8 ($13.5\ 10^{-2}$)[d]	-3.79 (-3.73)[d] -3.74 (-3.68)[e]

[a] The second harmonic vibrational frequency corresponds to a bending motion. The ZPE is given in parentheses in eV.
[b] The PUMP4[21] and CASPT2 *ab initio* calculations were performed using the 6-311G(2d) and aug-cc-pVTZ basis sets, respectively. Energies including the ZPE are given in parentheses and the zero of energy is taken in reactants.
[c] Ref. 21.
[d] Ref. 38. [e] Ref. 39 where the error in E can be estimated as ±0.38 eV, independently of the inclusion or not of the ZPE.
[f] In Ref. 21 no attention was devoted to the shallow minima MIN1 and MIN2 ($1^3A'$) of the PES. Moreover, MIN2 ($1^3A'$), which is placed $-3.95\ 10^{-2}$ eV with respect to products, connects with them after overcoming a barrier of $19.0\ 10^{-2}$ eV with respect to it (TS exit valley structure: R_e(OC)=1.1436 Å, R_e(CS)=3.5140 Å, and <OCS=180º; and vibrational frequencies of 93.4i, 90.61 (degenerate), and 2290.9 cm^{-1}), which is not found at the CASPT2 level.
[g] These frequencies were really calculated at the UMP4 level.[21]
[h] The energies of the CASPT2 MIN2 ($1^3A'$) and MIN2 ($1^3A''$) with respect to products are $-5.81\ 10^{-2}$ and $-6.16\ 10^{-2}$ eV, respectively.

Table II. QCT and TST rate constants for O + CS → CO + S on the $1^3A'$ and $1^3A''$ PESs, and TST and experimental total rate constants, expressed in units of 10^{12} $cm^3 \cdot mol^{-1} \cdot s^{-1}$.

T / K	$k(1^3A')$ [a]				$k(1^3A'')$ [a]	k	k
	TST/Wigner [b] (CASPT2)	QCT [c] (PUMP4 Anal. PES)	TST [d] (PUMP4 Anal. PES)	QCT [e] (MNDO/CI Anal. PES)	TST/Wigner [b] (CASPT2)	TST/Wigner [b] (CASPT2)	Experimental [f]
100	0.43	0.43	0.27 (0.45)		0.16	0.59	
150	1.29	0.74	0.70 (0.88)		0.80	2.10	1.02
175	1.82	0.94	0.91 (1.15)		1.31	3.12	2.11
200	2.37	1.13	1.13 (1.29)		1.90	4.28	3.64
225	2.95	1.35	1.34 (1.55)		2.58	5.53	5.55
250	3.54	1.58	1.55 (1.69)		3.32	6.86	7.77
275	4.14	1.73	1.77 (1.96)		4.10	8.25	10.3
300	4.75	1.95	1.98 (2.08)	0.12 (0.40)	4.93	9.68	12.9 [g]
500	9.72	3.38	3.57 (3.61)	0.39 (1.20)	12.41	22.13	
800	17.27	5.38	5.88 (5.88)	1.02 (3.10)	24.74	42.01	
1000	22.31	6.52	7.42 (7.40)	1.52 (4.60)	33.22	55.54	
1500	34.94	8.93	11.25 (11.21)		54.75	89.69	
2000	47.57	11.39	15.07 (15.03)		76.46	124.03	

[a] The TST, TST/Wigner, and QCT rate constants on the different PESs are multiplied by the electronic factor f_{el}, unless otherwise indicated. See eq. (3).

[b] The TST/Wigner results of this paper are essentially coincident with the TST ones. See text.

[c] QCT results of this paper.

[d] TST results from Ref. 21 (where the same analytical ground PES used here was employed) modified with the electronic factor of eq. (3). In parentheses are showed the values according to Ref. 21, where $f_{el} = 1/3$ was used.

[e] QCT results from Ref. 19 modified with the electronic factor of eq. (3). In parentheses are showed the values reported in Ref. 19, where $f_{el} = 1$ was used.

[f] Recommended values given in Ref. 18, which are essentially coincident with those derived from the Arrhenius fit of the experimental data (Ref. 17). The experimental error margins are reported in the text and in Figure 2.

[g] Experimental data at ~300 K appear to be well established (in $cm^3 \cdot mol^{-1} \cdot s^{-1}$): 13×10^{12} (298 K),[14] $12.4 \pm 0.84 \times 10^{12}$ (305 K),[15] $13.5 \pm 2.2 \times 10^{12}$ (300 K),[16] and 12.9×10^{12} (294 K),[17] where the lowest and highest values measured at T=294 K in Ref. 17 were 9.6×10^{12} and 15.7×10^{12}, respectively.

Table III. QCT average fractions of translational, vibrational, and rotational energy of the CO + S products on the 1^3A' PES.[a]

E_T / eV	T_{vr} = 300 K			T_{vr} = 1500 K		
	$\langle f_T' \rangle$	$\langle f_V' \rangle$	$\langle f_R' \rangle$	$\langle f_T' \rangle$	$\langle f_V' \rangle$	$\langle f_R' \rangle$
0.075	0.15	0.81	0.04	0.15	0.80	0.05
0.3	0.16	0.79	0.05	0.16	0.78	0.06
1.0	0.24	0.70	0.06	0.24	0.68	0.08
2.0	0.33	0.55	0.12	0.33	0.54	0.13

[a] The $\langle f_V' \rangle$ fraction includes the ZPE of the CO molecule.

FIGURE CAPTIONS

Figure 1 (color suggested).

Schematic representation of the energy profile along the MEP of the O + CS → CO + S reaction for the CASPT2 1^3A' and 1^3A" PESs and for the analytical 1^3A' PES. The MIN and TS energies are not plotted at scale to make them more easily evident.

Figure 2 (color suggested).

Arrhenius's plot of the O + CS → CO + S rate constants: a) CASPT2 $k_{TST}(1^3A')$, $k_{TST}(1^3A")$, and total k_{TST} values including tunneling (solid lines in red, blue, and black, respectively); b) Total k_{VTST} values including tunneling from the best data of Ref. 21 (dotted line in violet); c) Same as in b) but taking into account the electronic factor as described in eq. (3) (dotted line in green); d) Experimental data (circles), where empty and solid circles refer to measurements based on CO and CS detection, respectively,[17] and the uncertainties are defined by the dashed points lines.[18] The best total k_{VTST} results of Ref. 21 were obtained using the analytical ground PES and estimating the contribution to reactivity of the first excited PES.

Figure 3 (color suggested).

QCT (1^3A') cross section for O + CS → CO + S as a function of collision energy and at several rovibrational temperatures of CS [300 K (squares), 1000 K (rhombus) and 1500 K (circles)].

Figure 4 (color suggested).

QCT (1^3A') CO(v') vibrational state distributions from O + CS → CO + S at several collision energies and rovibrational temperatures of CS [300 K (squares), 1000 K (rhombus) and 1500 K (circles)]. Populations are normalized to unity.

Figure 5 (color suggested).

CO(v') vibrational state distributions from thermal O + CS reactants at T=300 K: Present QCT (1^3A') results (black solid squares), QCT (1^3A') results on an empirical LEPS PES[10] (red circles), and experimental data[3] (blue circles). Population in the maximum of the distribution is taken as unity.

Figure 6 (color suggested).

QCT (1^3A') (black) and experimental (squares)[10] CO(v'=12 and 14, j') rotational state distributions from the reaction at T=300 K (a)-(b). QCT (1^3A') (black (E_T =0.1 eV) and blue (E_T =0.2 eV)) and experimental[10] (squares; E_T distribution with peaks at 0.13 and 0.26 eV) CO(v'=12 and 14, j') rotational state distributions from the reaction at T_{vr}=300 K (c)-(d). The red curves in (a) and (b) correspond to the CO simulated rotational thermal distributions at 1507 and 2802 K, respectively; and the red curves in (c) and (d) correspond to a rotational distribution at 2802 K. Population in the maximum of the distributions is taken as unity.

Figure 7 (color suggested).

QCT (1^3A') angular distributions corresponding to the **kk'** (a, b), **kj'** (c, d), and **k'j'** (e, f) angles, at several collision energies [0.075 eV (circles), 0.3 eV (rhombus), 1.0 eV (squares), and 2.0 eV (triangles)] and two rovibrational temperatures of CS (300 and 1500 K).

Figure 8 (color suggested).

QCT ($1^3A'$) angular distribution corresponding to the **kk'j'** dihedral angle, at several collision energies [0.075 eV (circles), 0.3 eV (rhombus), 1.0 eV (squares), and 2.0 eV (triangles)] and two rovibrational temperatures of CS [300 K (a) and 1500 K (b)].

Figure 9 (color suggested).

Internuclear distances (R_{ij}) as a function of time [O-C (black), O-S (red), and C-S (blue) distances] for the types of reactive trajectories found for O + CS → CO + S on the $1^3A'$ PES: Direct (a), non-direct (b), and complex (c). The types (b) and (c) lead to the formation of short-lived and long-lived collision complexes, respectively. The types of trajectories (a)-(c) can also be found in the non-reactive case (see, e.g., a non-reactive long-lived collision complex in (d)).

Figure 1

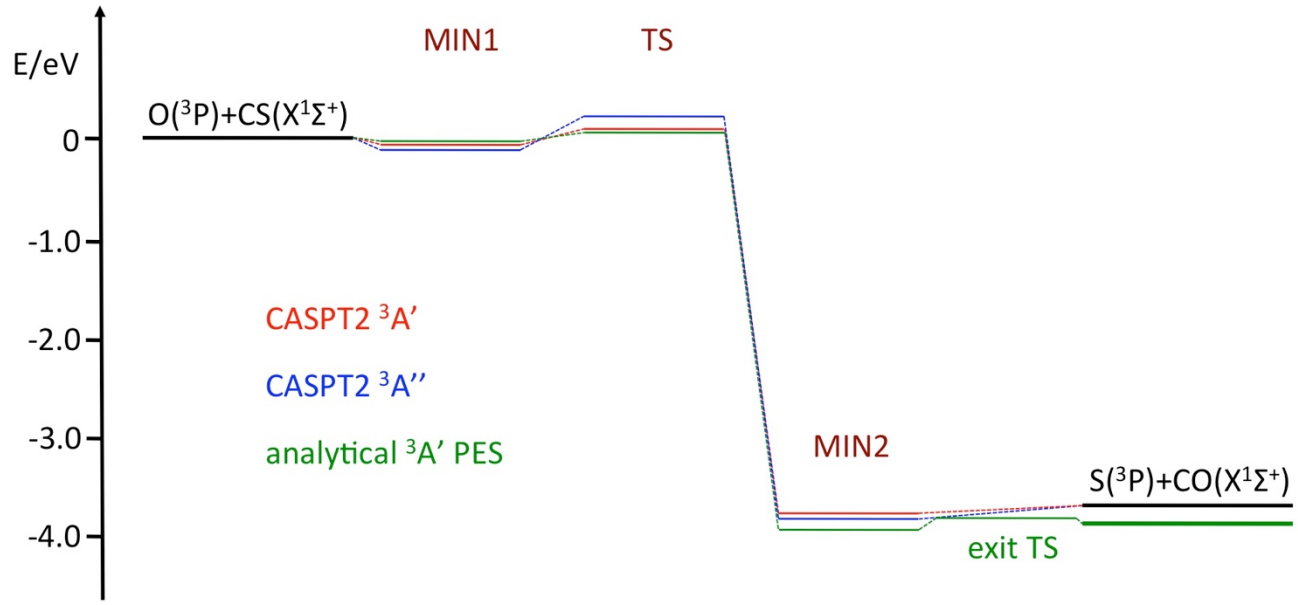
E/eV
0
-1.0
-2.0
-3.0
-4.0
O(3P)+CS(X1Σ+)
MIN1
TS
MIN2
S(3P)+CO(X1Σ+)
exit TS
CASPT2 3A'
CASPT2 3A''
analytical 3A' PES

Figure 2

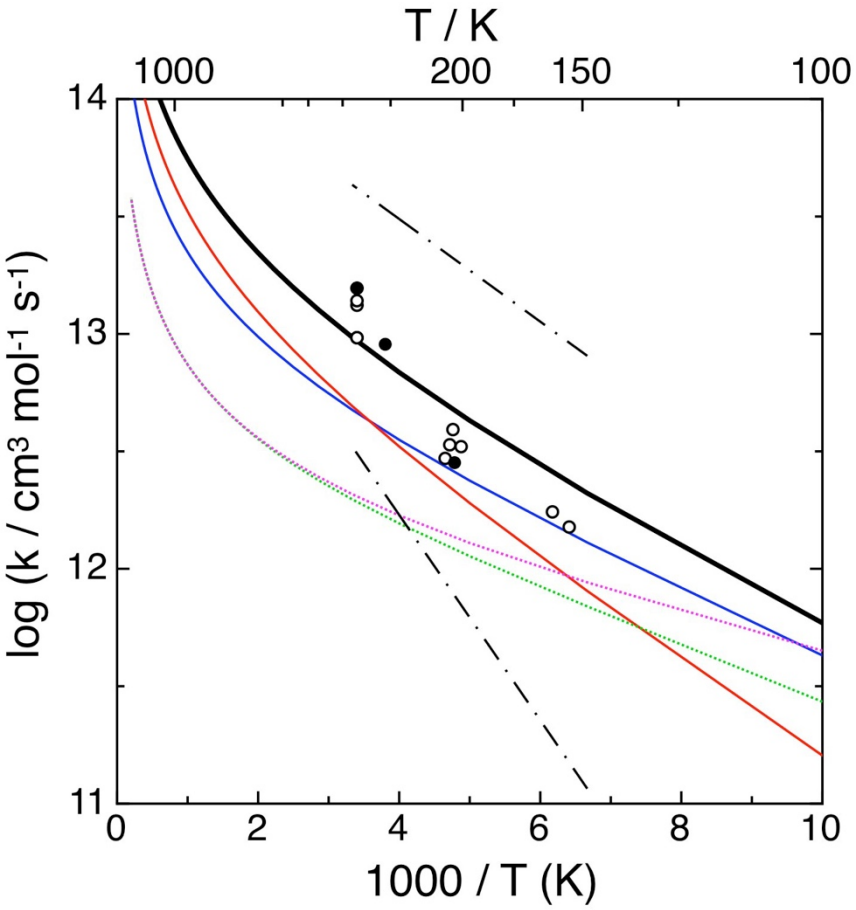

Figure 3

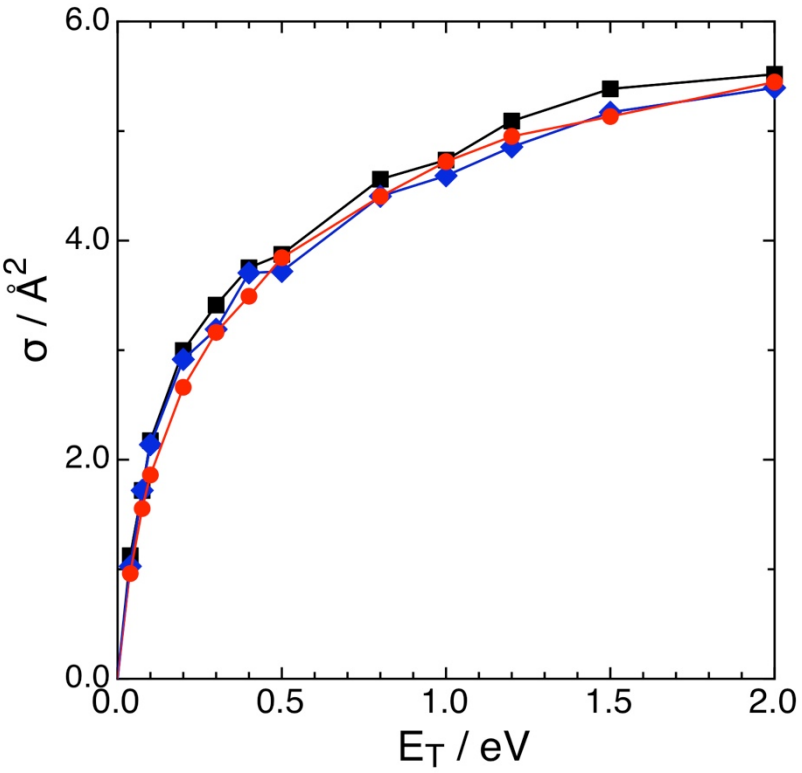

Figure 4

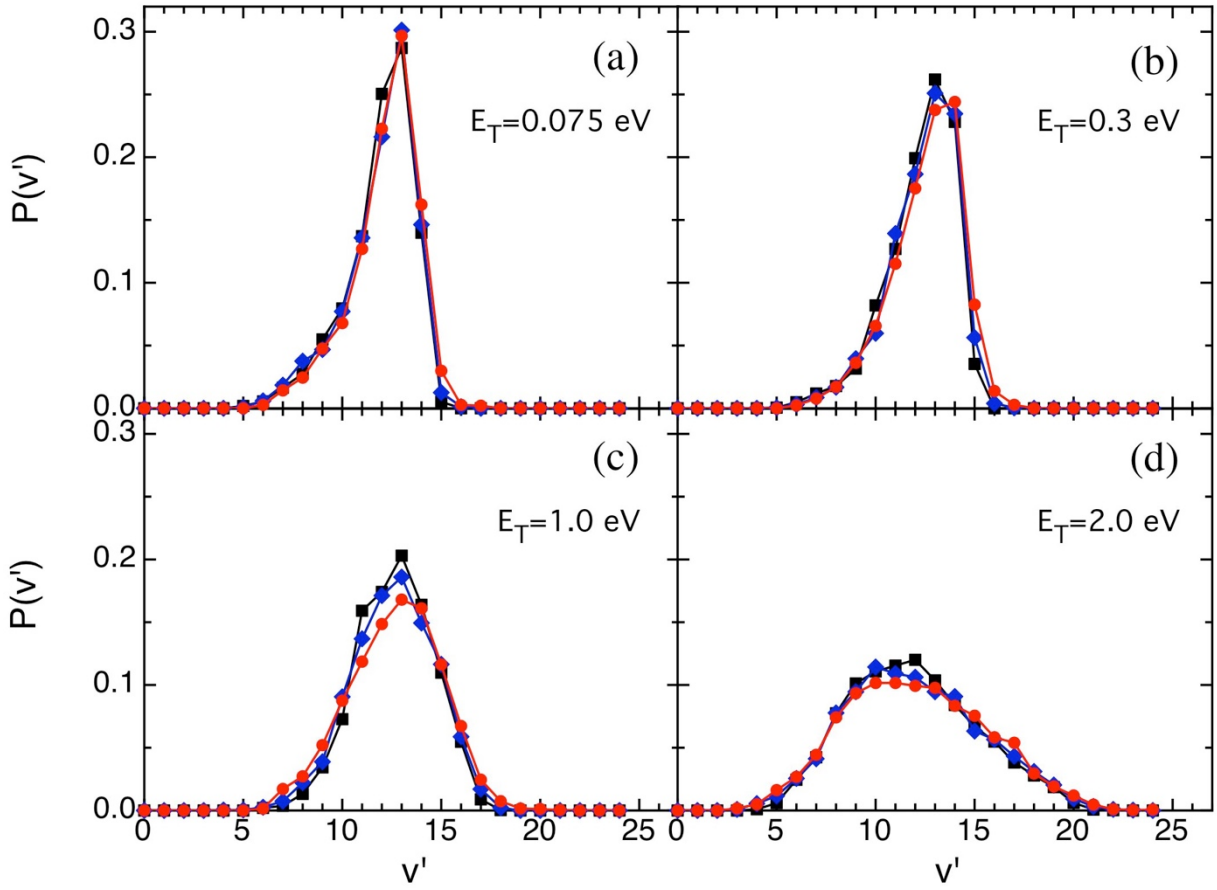
(a)
E_T=0.075 eV
(b)
E_T=0.3 eV
(c)
E_T=1.0 eV
(d)
E_T=2.0 eV
P(v')
P(v')
v'
v'
0.0
0.1
0.2
0.3
0
5
10
15
20
25

Figure 5

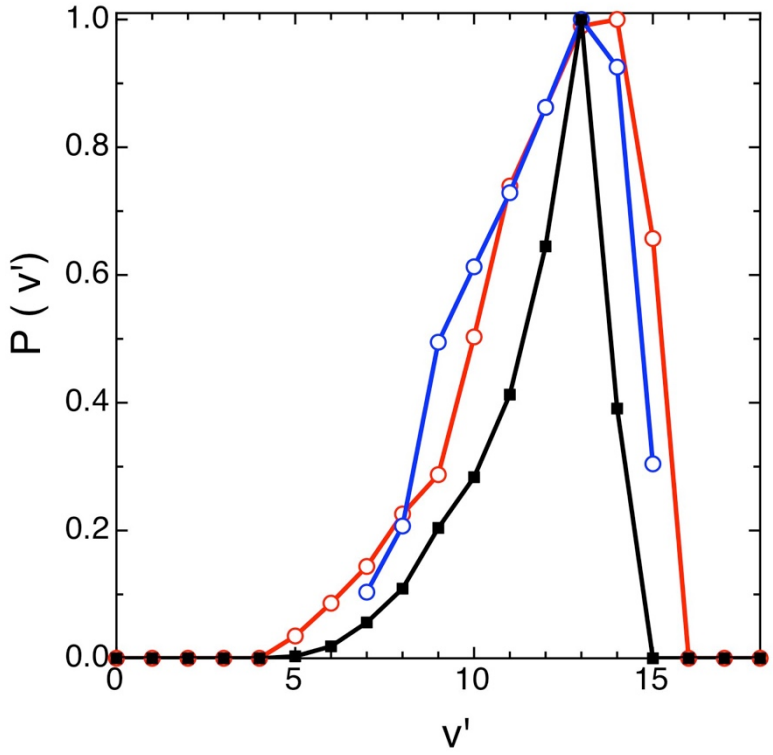

Figure 6

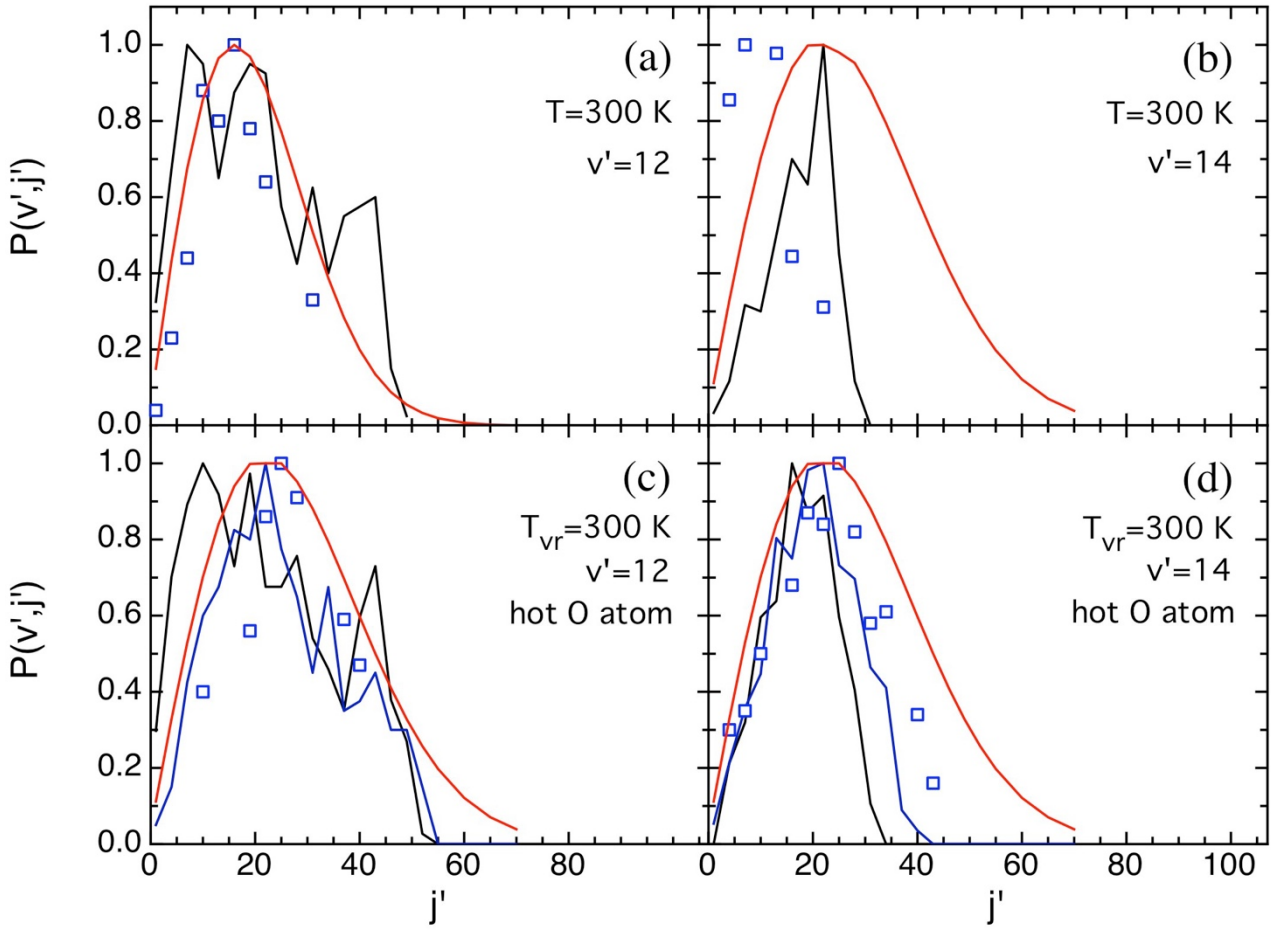
(a)
T=300 K
v'=12
(b)
T=300 K
v'=14
(c)
T$_{vr}$=300 K
v'=12
hot O atom
(d)
T$_{vr}$=300 K
v'=14
hot O atom
P(v';j')
P(v';j')
j'
j'
0.0
0.2
0.4
0.6
0.8
1.0
0
20
40
60
80
100

Figure 7

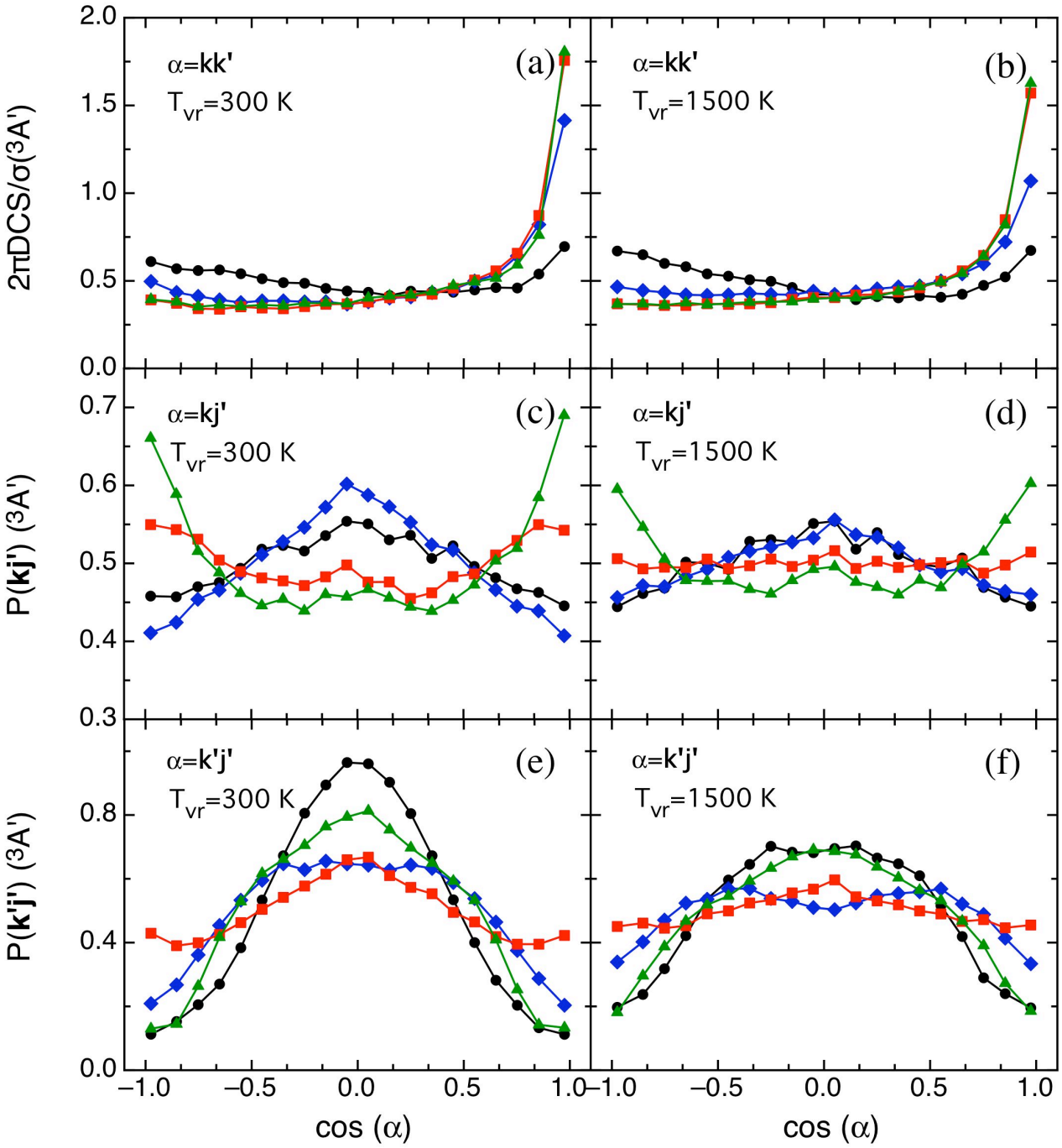
α=kk'
T_vr=300 K
(a)
α=kk'
T_vr=1500 K
(b)
α=kj'
T_vr=300 K
(c)
α=kj'
T_vr=1500 K
(d)
α=k'j'
T_vr=300 K
(e)
α=k'j'
T_vr=1500 K
(f)
2πDCS/σ(³A')
P(kj') (³A')
P(k'j') (³A')
cos (α)
cos (α)

Figure 8

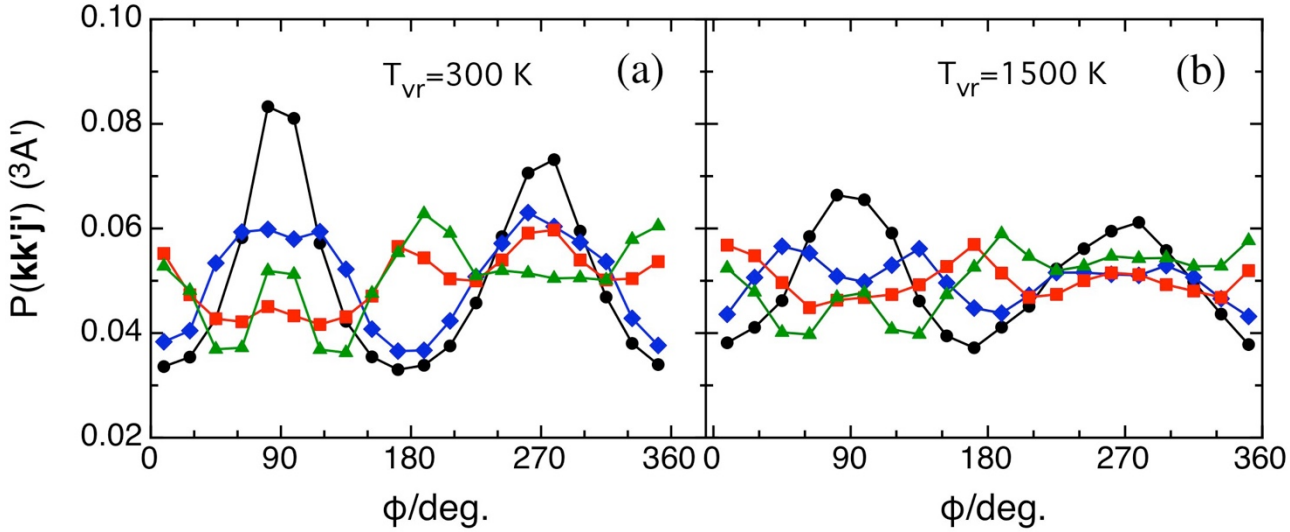
0.10
0.08
0.06
0.04
0.02
P(kk'j') (3A')
T_vr=300 K
(a)
T_vr=1500 K
(b)
0
90
180
270
360
ϕ/deg.

Figure 9

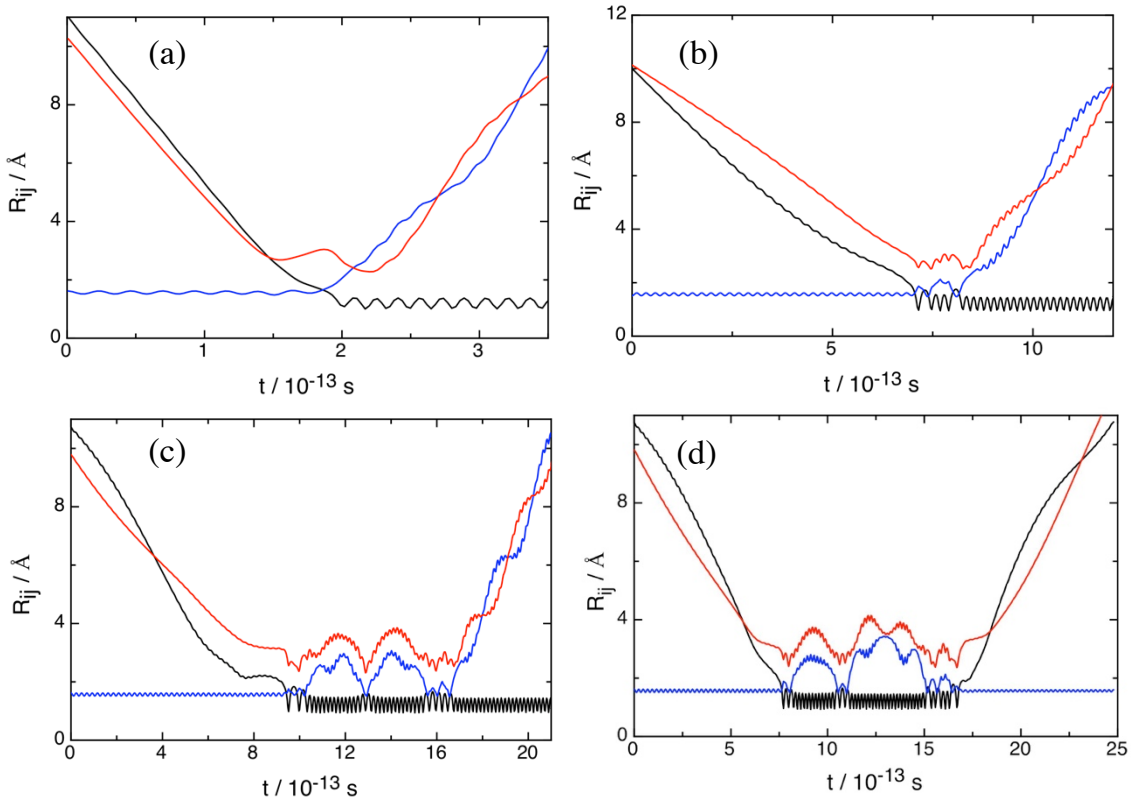

TOC graphic

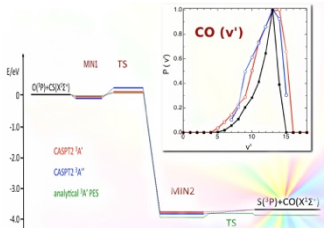

REFERENCES

[1] NIST-JANAF *Thermochemical Tables* (http://kinetics.nist.gov/janaf/).

[2] Pollack, M. A. *Appl. Phys. Lett.* **1966**, *8*, 237-238.

[3] Hancock, G.; Ridley, B. A.; Smith, I. W. M. *J. Chem. Soc. Farad. II.* **1972**, *68*, 2117-2126.

[4] Foster, K. D. *J. Chem. Phys.* **1972**, *57*, 2451-2455.

[5] Tsuchiya, S.; Nielsen, N.; Bauer, S. H. *J. Phys. Chem.* **1973**, *77*, 2455-2464.

[6] Powell, H. T.; Kelley, J. D. *J. Chem. Phys.* **1974**, *60*, 2191-2192.

[7] Djeu, N. *J. Chem. Phys.* **1974**, *60*, 4109-4115.

[8] Hudgens, J. W.; Gleaves, J. T.; McDonald, J. D. *J. Chem. Phys.* **1976**, *64*, 2528-2532.

[9] Hsu, D. S. Y.; Shaub, W. M.; Burks, T. L.; Lin, M. C. *Chem. Phys.* **1979**, *44*, 143-150.

[10] Summerfield, D.; Costen, M. L.; Ritchie, G. A. D.; Hancock, G.; Hancock, T. W. R.; Orr-Ewing, A. J. *J. Chem. Phys.* **1997**, *106*, 1391-1401.

[11] Green, F.; Hancock, G.; Orr-Ewing, A. J.; Brouard, M.; Duxon, S. P.; Enríquez, P. A.; Sayós, R.; Simons, J. P. *Chem. Phys. Lett.* **1991**, *182*, 568-574.

[12] Green, F.; Hancock, G.; Orr-Ewing, A. J. *Faraday Discuss. Chem. Soc.* **1991**, *91*, 79-90.

[13] Costen, M. L.; Hancock, G.; Orr-Ewing, A. J.; Summerfield, D. *J. Chem. Phys.* **1994**, *100*, 2754-2764.

[14] Hancock, G; Smith, I. W. M. *Trans. Faraday Soc.* **1971**, *67*, 2586-2597.

[15] Slagle, I. R.; Graham, R. E.; Gilbert, J. R.; Gutman D. *Chem. Phys. Lett.* **1975**, *32*, 184-186.

[16] Bida, G. T.; Breckenridge, W. H.; Kolln, W. S. *J. Chem. Phys.* **1976**, *64*, 3296-3302.

[17] Lilenfeld, H. V.; Richardson, R. J. *J. Chem. Phys.* **1977**, *67*, 3991-3997.

[18] Atkinson, R.; Baulch, D. L.; Cox, R. A.; Crowley, J. N.; Hampson Jr, R. F.; Hynes, R. G.; Jenkin, M. E.; Rossi, M. J.; Troe, J. *Atmos. Chem. Phys.* **2004**, *4*, 1461-1738.

[19] Sayós, R.; González, M.; Aguilar, A. *Chem. Phys.* **1990**, *141*, 401-415.

[20] Hijazo, J.; González, M.; Sayós, R.; Novoa, J. J. *Chem. Phys. Lett.* **1994**, *222*, 15-24.

[21] González, M.; Hijazo, J.; Novoa, J. J.; Sayós, R. *J. Chem. Phys.* **1996**, *105*, 10999-11006.

[22] Raff, L. M.; Thompson, D. L. In *Theory of Chemical Reaction Dynamics*; Baer, M., Ed.; CRC: Boca Raton, U.S.A., 1985; Vol. 3, p. 1-121.

[23] Mayne, H. R. *Int. Rev. Phys. Chem.* **1991**, *10*, 107-121.

[24] Miquel, I.; Hernando, J.; Sayós, R.; González, M. *J. Chem. Phys.* **2003**, *119*, 10040-10047.

[25] Gamallo, P.; Martínez, R.; Sayós, R.; González, M. *J. Chem. Phys.* **2010**, *132*, 144304:1-9.

[26] Steinfeld, J. I.; Francisco, J. S.; Hase, W. L. *Chemical Kinetics and Dynamics*; Prentice Hall: Upper Saddle River, U.S.A., 1998.

[27] Allison, T. C.; Truhlar, D. G. In *Modern Methods for Multidimensional Dynamics Computations in Chemistry*; Thompson, D. L., Ed.; World Scientific: Singapore, 1998; p. 618-672.

[28] Roos, B. O.; Taylor, P. R.; Siegbahn, P. E. M. *Chem. Phys.* **1980**, *48*, 157-173.

[29] Andersson, K. *Theor. Chim. Acta* **1995**, *91*, 31-46.

[30] Gamallo, P.; González, M.; Sayós, R. *J. Chem. Phys.* **2003**, *118*, 10602-10610.

[31] Brouard, M.; Quadrini, F.; Vallance, C. *J. Chem. Phys.* **2007**, *127*, 084305:1-12 and references cited therein.

[32] Murrell, J. N.; Carter, S.; Farantos, S. C.; Huxley, P.; Varandas, A. J. C. *Molecular Potential Energy Functions*, John Wiley & Sons: Chichester, U.K., 1984.

[33] Karlström, G.; Lindh, R.; Malmqvist, P.-Å.; Roos, B. O.; Ryde, U.; Veryazov, V.; Widmark, P.-O.; Cossi, M.; Schimmelpfennig, B.; Neogrady, P.; Seijo L. *Comput. Mater. Sci.* **2003**, *28*, 222-239.

[34] Sansonettia, J. E.; Martin, W. C. *J. Phys. Chem. Ref. Data* **2005**, *34*, 1559-2257.

[35] Matzkies, F.; Manthe, U. *J. Chem. Phys.* **1998**, *108*, 4828-4836.

[36] Manthe, U.; Capecchi, G.; Werner, H.-J. *Phys. Chem. Chem. Phys.* **2004**, *6*, 5026-5030.

[37] Bonnet, L.; Rayez, J.-C. *Chem. Phys. Lett.* **1997**, *277*, 183.

[38] Huber, K. P.; Herzberg, G. *Molecular Spectra and Molecular Structure. IV. Constants of Diatomic Molecules*; Van Nostrand Reinhold: New York, U.S.A., 1979.

[39] Reddy, R. R.; Ahammed, Y. N.; Gopal, K. R.; Basha, D. B. *Astrophys. Space Sci.* **2003**, *286*, 419–436.

[40] Azizi, Z.; Roos, B. O.; Veryazova, V. *Phys. Chem. Chem. Phys.* **2006**, *8*, 2727–2732.

[41] Levine, R. D.; Bernstein, R. B. *Molecular Reaction Dynamics and Chemical Reactivity*, Oxford University Press: Oxford, 1987.

[42] Aoiz, F. J.; Brouard, M.; Enríquez, P. A. *J. Chem. Phys.* **1996**, *105*, 4964-4982.

[43] Kim, S. K.; Herschbach, D. R. *Faraday Discuss. Chem. Soc.* **1987**, *84*, 159-169.